Laser Processing of $La_{61.4}Al_{15.9}Ni_{11.35}Cu_{11.35}$ Based Functionally Graded Material Bulk Metallic Glass

Qayyum Halim, Nik Abdullah Nik Mohamed, Mohd Ruzaimi Mat Rejab, Mohd Kamal Kamarulzaman, Sakinah Hisham, and A. M. Aizzuddin

Abstract Bulk metallic glass (BMG) based on lanthanum is one of the BMG with exceptional glass-forming ability (GFA). The $La_{61.4}Al_{15.9}Ni_{11.35}Cu_{11.35}$ bulk metallic glasses were treated to a laser processing test in this experiment. The results showed that the best power, frequency, and speed ranges for laser processing of the $La_{61.4}Al_{15.9}Ni_{11.35}Cu_{11.35}$ BMG samples are 40–50 W, 160–240 kHz, and 200–400 mm/s, respectively. As a result, the current work was effective in producing the Lanthanum-based functionally graded material (FGM) BMG. The positive findings on the laser's microstructural or morphology, give a solid foundation for future advancement research on the $La_{61.4}Al_{15.9}Ni_{11.35}Cu_{11.35}$ BMG.

Keywords La-based BMG · Functionally graded material bulk metallic glass · Laser processing

1 Introduction

Metallic glass (MG) is an advanced engineered material with several crucial processes. The first known successful development of bulk metallic glass (BMG) is from Klement et al. from California Technology Institute in 1950–1960 [1–3]. Ruhl et al. team from the Massachusetts Institute of Technology makes additional BMG findings later [4–6]. The known Metallic Glass (MG) was in the ribbon form

Q. Halim · N. A. N. Mohamed · M. R. M. Rejab · S. Hisham
Faculty of Mechanical and Automotive Engineering Technology, Universiti Malaysia Pahang, 26600 Pekan, Pahang Darul Makmur, Malaysia

M. K. Kamarulzaman (✉)
Advanced Nano Coolant-Lubricant (ANCL) Lab, Automotive Engineering Centre, Universiti Malaysia Pahang, 26600 Pekan, Pahang Darul Makmur, Malaysia
e-mail: kamalkz@hotmail.com

A. M. Aizzuddin
College of Engineering, Universiti Malaysia Pahang, 26600 Pekan, Pahang Darul Makmur, Malaysia

N. H. Johari et al. (eds.), *Proceedings of the 2nd Energy Security and Chemical Engineering Congress*, Lecture Notes in Mechanical Engineering,
https://doi.org/10.1007/978-981-19-4425-3_28

and only 1 mm in thickness size. Akihisa Inoue et al. from Tohoku University has made MG samples from different elements (Al, La, Fe, Ni, Cu, Ag and Sn) and lists out their glass-forming ability (GFA) [7, 8]. Later the MG creation method was able to be produced in bulk (more than 1 mm thickness), which uses the copper block to supercool (super-cooling time of $1-10^1$ K/s [9] the molten MG elements. Previous alloy system that is less than three elements system have the super-cooling time of 10^3-10^5 K/s [10]. Lower super-cooling time will reduce the effect of stress from rapid cooling, resulting in fracturing. Other methods are also found in the creation of BMG (Exceeding 1 mm thickness). In the latest trend, Ouyang et al. [10] used the selective laser melting 3D metal printer to produce BMG with better shape complexity. This opens up the possibility for BMG to be used in rapid prototyping parts for practical usage. On the other hand, a Lanthanum based BMG as the chosen sample in this work is an alternative for the lightweight alloy. The base metal is abundant and has an excellent glass-forming ability (GFA) for the BMG.

1.1 Ductilisation Studies on BMG

The common understanding of BMG agrees that the ductility of BMG is lower compared to conventional alloys. Although that is the case, studies on how to enhance BMG ductility is continuing. The author has compiled in Table 1 the ductilisation-related research regarding the BMG alloy systems, processes and Young's modulus values that can be a valuable reference for other BMG ductilisation research [3].

Hence, to describe ductility in a comprehensive method, it is agreeable that more properties information is needed [11]. Information such as shear modulus, bulk modulus, alloy's density, and Poisson's ratio are needed to derive a comprehensive conclusion [12]. Nevertheless, as for benchmarking purposes of BMG ductilisation, Young's modulus (stiffness) is inversely proportional to the actual ductility value of BMG samples [13, 14]. It can be beneficial information when the research of localised ductilisation and characterisation of functionally graded material (FGM) bulk metallic glass (BMG) is initiated.

Table 1 Compilation of data from ductilisation-related research in terms of the BMG alloy systems, processes and Young's modulus, E

BMG alloy system	Process	E (GPa)	Refs.
Pt–Cu–Ni–P	Compression, bending	94.8	[12]
Cu–Zr	Compression	84	[15]
Zr–Al–Ni–Cu–Ti	Cold rolling	82	[16]
Ti–Zr–Cu–Be–V	Tensile, nanoindentation	94.2	[17]
Ti–Zr–Nb–Cu–Be–Sn	Nanoindentation	120.3	[18]
Zr–Ti–Cu–Ni–Al	Imprinting	105	[19]
La–Al–Ni–Cu	Compression, bending	25	[20]

1.2 Localised Ductilisation of the Bulk Metallic Glass (BMG)

Investigation of the re-scanning method to prevent macro-cracks during selective laser melting (SLM) of $Al_{85}Ni_5Y_6Co_2Fe_2$ bulk metallic glass composites (BMGC's) had been presented by Li et al. [21]. The crack was caused by residual stress of rapid heating and cooling during SLM. BMGC's possess supercooled liquid regions that can release stress by plastic flow. It was shown that high power initial scan for material melting followed by a lower power re-scan for stress relief was able to prevent cracking. A crack free $Al_{85}Ni_5Y_6Co_2Fe_2$ BMGC's was created with gear design. The diameter is ~25 mm and height ~10 mm [21].

Additive manufacturing can produce bulk metallic glass (BMG) with good design and sizes. The major challenge of creating BMG using additive manufacturing is micro-cracking. It is caused by substantial thermal stress in the process, particularly around the micro-pores. Thus, degrade the mechanical performance of the parts created. Systematic experiments and finite element simulation on Fe-based metallic glass, which is intrinsically brittle was done. $Fe_{43.7}Co_{7.3}Cr_{14.7}Mo_{12.6}C_{15.5}B_{4.3}Y_{1.9}$ (at.%) have the excellent glass-forming ability (critical cooling rate for glass formation approximately at 80 K/s) and was chosen as the powder material base [22]. Using selective laser melting (SLM) with process optimization to avoid micro-cracks. Cu and CU-Ni alloy powder forming BMG composites were introduced to subdue the development of micro-cracks. Results have shown micro-crack reduction with high-density dislocation formation in the second phase of SLM. The second phase reduces thermal stress with the relaxation of strain energy. Fracture toughness of second phase Fe-based BMG improved to 47 MPa $m^{1/2}$ compared to first phase Fe-based BMG 2.2 MPa $m^{1/2}$. The SLM method for BMG development with composites can enhance mechanical properties while maintaining geometries of parts created [22].

Imprinted glass is considered an orthotropic material that possesses heterogeneous microstructures due to imprinting ductilisation. Consequently, the shear band dynamics and mechanical behaviour of the BMG would vary under compression or tensile loadings. Scudino et al. [19] studied the correlation between structural heterogeneities and shear bands morphology of a $Zr_{52.5}Ti_5Cu_{18}Ni_{14.5}Al_{10}$ BMG through experimental and computational methods. The effects of loading angle, α, on the tensile behaviour of the BMG samples were analyzed through the tensile tests. The results revealed that both strength and ductility improved when α was increased from 0 to 45° due to the shear band branching and deflection mechanisms [19].

Dong et al. [23] examined the ductility of Zr-based BMG having varied hydrogen content. The plasma-assisted hydrogenation method introduced hydrogen at varied content, and uniaxial compression tests were performed on the BMG rods. The results showed that hydrogen significantly improved the compressive properties, plasticity and ductility of the $Zr_{55}Cu_{30}Ni_5Al_{10}$ metallic glass.

Table 2 Functionally graded material (FGM) BMG alloy system, process, and aim of the study

BMG alloy system	Process	Aim of the study	Refs.
Zr–Ti–Cu–Ni–Al	Laser additive manufacturing (LAM)	Extending the applications of metallic glass for use as functionally graded	[24]
Zr–Ti–Cu–Ni–Al	Laser direct manufacturing (LDM)	LDM technology to fabricate structural-graded materials	[25]

1.3 Functionally Graded Material (FGM) Bulk Metallic Glass (BMG)

To the best of the author's knowledge, functionally graded material (FGM) bulk metallic glass (BMG) is still an area of research that is scarcely explored. Having stated this, an exploration of the niche area would benefit the future practical application of BMG. In Table 2, using laser additive manufacturing (LAM) and direct laser manufacturing (LDM) [3], the researchers aim to extend the BMG application as part of FGM [24, 25].

The author's research with literature support (Table 2) suggested that the FGM BMG would open up BMG capabilities to allow conventional alloy processes such as machining and joining. Similarly, with localised ductilisation using the laser method, various FGM BMG can be produced depending on usage.

1.4 Joining Process of BMG

The bulk metallic glass research area on the joining method is continuing until today. Admittedly, the maturity of BMG engineering would be to produce the part as cast rather than to join it. Although that is the case, Table 3 compiled various research on the joining of BMG [3]. The studies were done to further the general understanding of BMG on this subject matter. Consequently, this understanding comes from the meta-stability of the BMG that is vastly affected by the high-temperature procedure of joining the BMG [26]. Providing crucial information on annealing of the heat-affected zone (HAZ), joining ability, quality, and strength.

Importantly, by introducing a joining procedure to BMG with applying high temperature surpassing the eutectic point. Coupled it with an annealing process that happens by ambient temperature. Therefore will result in the crystalline reverting process of the BMG, which was subjected to the heat-affected zone (HAZ) [28].

The author has a hypothesis that using the laser processing method, the $La_{61.4}Al_{15.9}Ni_{11.35}Cu_{11.35}$ metallic glass can be processed to become a graded material. A proper study of graded material towards the $La_{61.4}Al_{15.9}Ni_{11.35}Cu_{11.35}$ metallic glass has not been done to the best of the author's knowledge. This is an excellent

Table 3 Joining of BMG alloys system, process, and aim of the study

BMG alloy system	Process	Aim of the study	Refs.
Zr–Cu–Ni–Al	Laser welding	Laser welding effect on annealed BMG	[27]
Zr–Cu–Al–Ni	Laser welding	Crystallisation effect of BMG in laser welding	[28]
Zr–Cu–Al–Ni	Friction stir welding (FSW)	FSW joining of BMG to alloy plates	[29]
Zr–Ti–Ni–Cu–Al	Friction stir welding (FSW)	Joining of BMG to aluminium alloy	[30]
Zr–Ti–Ni–Cu–Al, Zr–Cu–Ni–Al	Liquid–solid joining process	Joining two BMG using the solid–liquid process	[31]
Cu–Ni–Zr–Ti	Brazing	Joining BMG to carbon steel	[32]

opportunity to closing the gap of expanding the size and application of the metallic glass, specifically for the $La_{61.4}Al_{15.9}Ni_{11.35}Cu_{11.35}$ metallic glass [33].

2 Materials and Methods

2.1 Samples Preparation

The $La_{61.4}Al_{15.9}Ni_{11.35}Cu_{11.35}$ BMG was obtained through an organization provides by Malaysia's Ministry of Science, Technology, and Innovation (MOSTI): 03-01-02-SF0257. To eliminate the thermal history from the prior cutting operation, the $La_{61.4}Al_{15.9}Ni_{11.35}Cu_{11.35}$ BMG samples were manually surface ground using 240, 320, 400, and lastly 640 grid sandpaper. Additionally, to achieve a flat surface for laser processing, the surface roughness must be reduced.

2.2 Localised Heating Process

A conceptualize method to gain localised ductilisation on the BMG samples can be observed from Fig. 1. BMG area at the heat-affected zone (HAZ) from the suggestive laser heating process will crystallize after annealing. The targeted heat applied to reach the crystalline temperature (T_x) of the Lanthanum based BMG that is 417 K. This is still lower from the melting temperature (T_g) of 446 K, with the different temperature of (ΔT) 29 K. When annealed at ambient room temperature, the localised heating area such as Fig. 1 will make the area ductile, which revert to conventional metallic properties [28, 34].

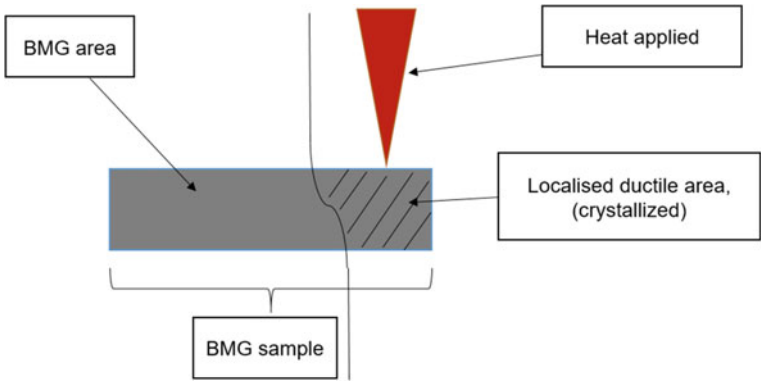

Fig. 1 Illustration of the sample with localised ductilisation

The laser machine of CK-FB3D Laser 3D Fiber Laser Marking Cutting Marking Engraving Machine located Kolej Kemahiran Tinggi MARA Kuantan was used in this study. The machine, laser parameters need to be taken into account, such as pulse or continuous, the thermal conductivity of samples, temperature to heat up, laser speed, laser power, et cetera [27, 35, 36]. Setting up the laser run for the BMG samples is crucial to obtain the best laser parameters to achieve suitable localised heating.

Table 4 shows the compilation of studies on the localised heating of the BMG in terms of the alloys system, process, and aim of the study. These references make the idea generated from the aim of studies, using the laser process to create a localised ductilisation, plausible. By selecting the proper parameter and method of laser process, combined with annealing at ambient temperature, the creation of a localized ductilisation has been proven.

Table 4 Compilation of studies on the localised heating of the BMG in terms of the alloys system, process, and aim of the study

BMG alloy system	Process	Aim of the study	Refs.
Zr–Al–Ni–Cu	Diode laser	Crystallisation effect by laser	[37]
Zr–Ti–Cu–Ni–Be	Single-pulse ablation laser	Explosive boiling of MG superheated by nanosecond pulse laser ablation	[38]
Zr–Ti–Cu–Ni–Be	Nanosecond laser (Yb laser fibre)	Generating micro-scale features on BMG	[35]
Zr–Be–Ti–Cu–Ni	Nanosecond laser	Morphology study of BMG from nanosecond laser	[34]
Zr–Cu–Ni–Al	Laser welding	Characteristics of the weld structure in the heat-affected zone and the fusion zone	[14]

Other methods that are in the back-burner by the author are hot oil quenching of the BMG samples. Another method is conventional controlled localised heating by a blow torch. Both of these localised heating methods are the author's original ideas.

The localised ductilisation process was done using the CK-FB3D Laser 3D Fiber Laser. The optimum laser parameters to be used on the La-based MG is selected after a thorough comparison from previous works on laser machine MG as compiled in Table 5. The previous researches were found to use the Zr-based and Al-based MG for the samples. While in this study, the author will recreate the laser processing into La-based MG. The following Table 6 shows the CK-FB3D Laser 3D Fiber Laser parameters, which are devised accordingly for this study.

Table 5 The comparison of parameters for BMG laser processing

Laser type	Laser power (W)	Speed (mm/s)	Frequency (kHz)	Material	Refs.
400 W Yb-fibre laser (SLM)	400	–	–	$Zr_{59.3}Cu_{28.8}Nb_{1.5}Al_{10.4}$	[39]
KrF excimer laser (PLD-IV)	–	–	–	$Zr_{47.7}Cu_{31}Ni_9Al_{12.3}$	[40]
Ns-pulsed laser	18	1900	100	$Zr_{52.5}Cu_{17.9}Ni_{14.6}Al_{10}Ti_5$	[41]
Diode laser	500	300	–	$Zr_{55}Al_{10}Ni_5Cu_{30}$	[37]
Fibre laser	200	625	–	$Al_{85}Ni_5Y_6Co_2Fe_2$	[21]
Nd: YAG laser	–	–	–	$Zr_{41.2}Ti_{13.8}Cu_{12.5}Ni_{10.0}Be_{22.5}$	[38]
LSF-IIIB laser	4000	200		$Zr_{55}Cu_{30}Al_{10}Ni_5$	[42]

Table 6 The default parameter of the CK-FB3D laser machine used in this project

Parameter	
Model	CK-FB3D
Output power	50 W
Depth of engraving (based on material)	<0.3 mm
Operating voltage	AC 220 V 50 Hz 5 A
Laser wavelength	1064 nm
Speed	1000 mm/s
Frequency	30 kHz
Pulse width	0 ns
Laser/on delay	750 µs
Laser/off delay	950 µs
End delay	100 µs
Polygon Tc	30 s

2.3 Characterisation of FGM BMG Samples

Planned functionally graded material (FGM) bulk metallic glass (BMG) samples to be produced will have a part of the samples be crystalline and a part of the samples to be amorphous. Taken into account this fact, the FGM BMG would produce two distinct properties in one sample. One area has high hardness but is inherently brittle, and one area has ductility but is lower in hardness. Characterisation of the ductile portion could be made through the microstructure observation using FESEM. A destructive test is allowable if the quantity of the sample produced was pre-planned. A uniaxial compressive (stress–strain) test, which is set to stop before the failure point to make the test not destructive, can produce a rate of stress–strain relation, which offers information of the FGM BMG behaviour.

2.4 Morphology Around Laser Response of the Lanthanum Based FGM BMG Samples

After the localised ductilisation process of lasering the La-based MG, the laser tracking of the samples was observed under the microscope. The laser parameters were varied by power percentage, frequency (kHz), and speed (mm/s). Overall, 20 laser tracks were observed under the JEOL JSM-7800F high-resolution Field Emission Scanning Electron Microscope (FESEM). With its 300,000 times magnification and fast graphic computation, the observation is suitable for this type of machine. The analysis of the results from the morphology around the laser response can be concluded for the best laser parameter for $La_{61.4}Al_{15.9}Ni_{11.35}Cu_{11.35}$ FGM BMG.

3 Results and Discussion

The rationale of a functionally graded material bulk metallic glass (FGM BMG) is that both advantageous properties occurring in crystalline and amorphous structures can be applied. An example of FGM BMG is from the research of Windl [43] for military usage, the development of compositionally graded metallic glass $Zr_{55}Al_{10}Ni_5Cu_{30}$ shows promising results as penetration bullet. Other than that, Yunzhuo et al. research showed how the $Zr_{50}Ti_5Cu_{27}Ni_{10}Al_8$ (Zr50) was used to create a gradual variation of crystallinity [24, 25]. This was mainly due to the gradient structural relaxation accumulation induced by the thermal history from laser additive manufacturing (LDM) [24, 25]. As far as the author's knowledge, there are a few or minimal sources of literature point at the FGM from the Lanthanum based BMG. The final Lanthanum, FGM BMG process, is planned to be as Fig. 1, where it is easy to point to which area for ductilisation for the specific application. To achieve this, further experiment and research on the $La_{61.4}Al_{15.9}Ni_{11.35}Cu_{11.35}$ sample needs to be done to

observe its response. Therefore, in current work, the successful production of the $La_{61.4}Al_{15.9}Ni_{11.35}Cu_{11.35}$ FGM BMG was a novelty that contributed to BMG knowledge. In current works, the results were promising to show the broad-spectrum laser parameter of the laser tracking process and its results from the FESEM point of view.

3.1 FESEM Results for FGM BMG

The FESEM of FGM BMG laser tracking results were essential for observing the heat-affected zone (HAZ) impact [25]. The different regions of amorphous and crystalline structure in one sample BMG as the laser processing occurred need to be analysed to see the best parameter for the laser tracking experiment [14].

Figure 2 of Wessels et al. [41] work showed the SEM images of the $Zr_{52.5}Cu_{17.9}Ni_{14.6}Al_{10}Ti_5$ BMG samples after the samples were applied, the direct laser track was run with various parameters. Wessels et al. [41] showed the explicit representation of the laser tracking in terms of the crystallisation and extreme surface

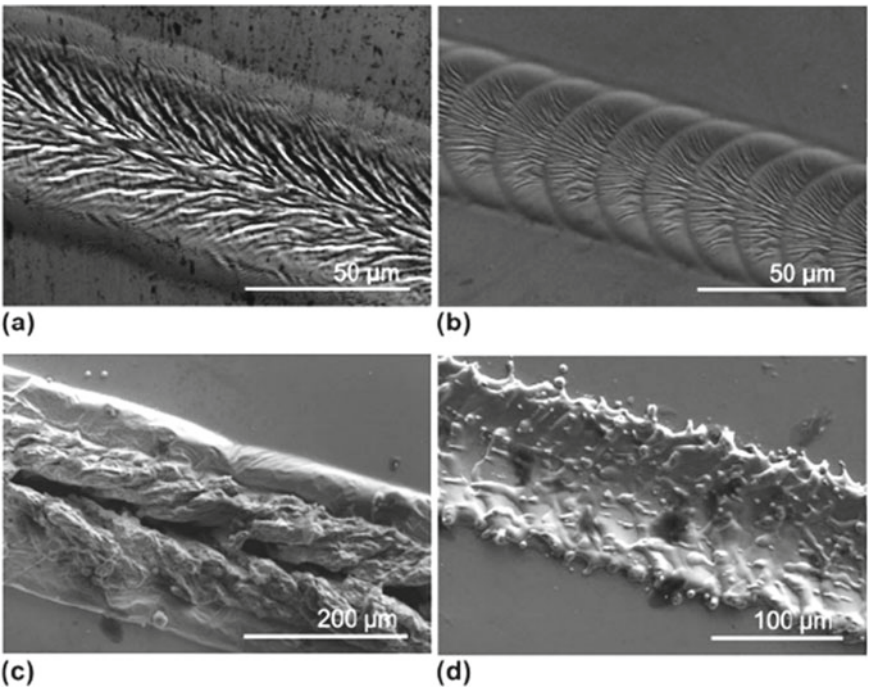

Fig. 2 Grooves engraved into the surface of the BMG by an ns-pulsed laser at **a**, **b** 100 and 1000 mm/s feed rates, respectively, and 10% power; **c**, **d** 100 and 1000 mm/s, respectively, and 70% power. In **a**, **b**, contraction due to crystallisation is indicated by the rippled morphology; in **c**, **d**, extreme surface damage and redeposition of melted material are seen. *Source* Wessels et al. [41]

damage on the BMG sample. An ns-pulsed laser engraved grooves into the surface of the BMG at (a, b) 100 and 1000 mm/s feed rates, respectively, and 10% power; (c, d) 100 and 1000 mm/s, respectively, and 70% power. The rippling morphology in (a, b) indicates contraction owing to crystallisation; in (c, d), significant surface damage and redeposition of melted material are seen.

In current work, the $La_{61.4}Al_{15.9}Ni_{11.35}Cu_{11.35}$ FGM BMG was synthesised as in the Wessels et al. [41] works of the laser tracking experiments. The laser can be controlled to be a pulse or continuous. Power penetration can be controlled high and low. Smaller localised heating can be used for the BMG samples. If the parameters are suitable, the percentage of the localised crystalline area on the BMG sample can be increased even further, and the qualitative data is synthesised. Table 5 is the selected compilation of the BMG laser processing parameters.

By compiling several laser processing parameters and analysing the work done by Wessels et al. [41], the laser experiment can be done with a reasonable degree of confidence. To the best of the author's knowledge, the $La_{61.4}Al_{15.9}Ni_{11.35}Cu_{11.35}$ FGM BMG by laser processing was not published before, and the specific parameters for the laser were also not available. Figures 3, 4 and 5 show the $La_{61.4}Al_{15.9}Ni_{11.35}Cu_{11.35}$ MG under laser tracking processes via the FESEM observation.

Figure 3 shows FESEM images response towards laser tracking with variations of power (W). A variation from 10 to 100% of power was done to the $La_{61.4}Al_{15.9}Ni_{11.35}Cu_{11.35}$ BMG. It can be concluded that the crystallisation of $La_{61.4}Al_{15.9}Ni_{11.35}Cu_{11.35}$ BMG can be completed in the 80, 90, and 100% of the

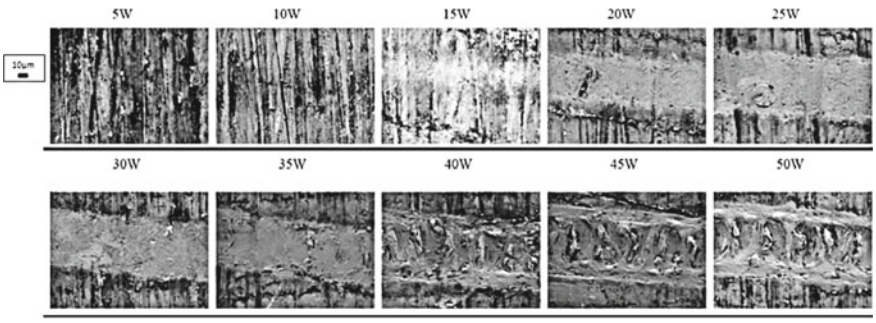

Fig. 3 The morphology of $La_{62}Al_{14}Cu_{12}Ni_{12}$ BMG samples after laser tracking process. The parameter power (W) was varied from 5 to 50 W with the increment of 5, equivalent to 10–100%

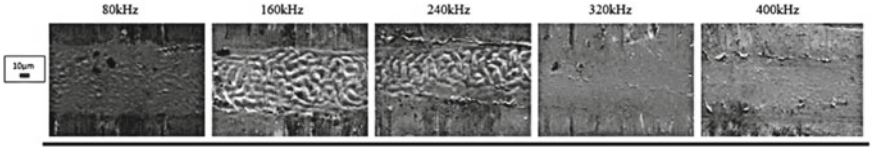

Fig. 4 The morphology of $La_{61.4}Al_{15.9}Ni_{11.35}Cu_{11.35}$ BMG samples after laser tracking process. The parameter frequency (kHz) was varied from 80 to 400 kHz

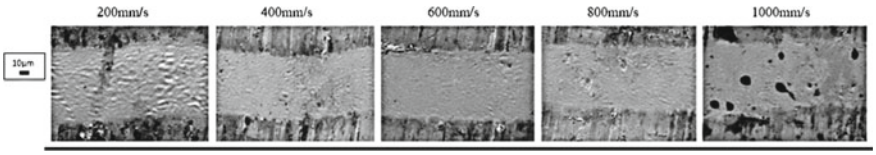

Fig. 5 The morphology of $La_{62}Al_{14}Cu_{12}Ni_{12}$ BMG samples after laser tracking process. The parameter speed (mm/s) was varied from 200 to 1000 mm/s

power penetration, which are equivalent to 40, 45 and 50 W. This is because the ripple patterns were evident in that region. The 70% power and lower shows no major ripple patterns and can be concluded that the HAZ does not reach the needed temperature to attain a heavy crystalline zone.

Figure 4 shows with the fixed setting of 50% power equal to 25 W, but variations of frequency, the $La_{61.4}Al_{15.9}Ni_{11.35}Cu_{11.35}$ demonstrates heavy ripple pattern creation using 160 and 240 kHz settings. Which translate to 40 and 60% of the frequency intervals. A conclusion of the best crystallisation occurrence with good HAZ happen at 160–240 kHz frequency region.

Figure 5 shows with fixed setting 50% of power equal to 25 W, but variations of speed, the $La_{61.4}Al_{15.9}Ni_{11.35}Cu_{11.35}$ demonstrates substantial ripple pattern creation with 200 and 400 mm/s modes. Which convert to 20 and 40% of the speed intervals. The most acceptable crystallisation existence with decent HAZ happens at 200–400 mm/s speed parameter region. Table 7 lists the optimum parameters for the $La_{61.4}Al_{15.9}Ni_{11.35}Cu_{11.35}$ BMG based on the FESEM observation.

Although the FESEM results were concluded intuitively for the $La_{61.4}Al_{15.9}Ni_{11.35}Cu_{11.35}$ BMG FGM parameters. Equation 1 shows the relation of heat (Q), specific heat (C_p), mass (m), and temperature change (ΔT). The simplified relation of heating from the laser towards the La-based BMG can show the crystallisation occurrence.

Heat and Energy relation.

$$Q = C_p \times m \times \Delta T \tag{1}$$

With 50 W of laser power, Lanthanum specific heat of 0.19 J/g K, the mass of the samples at 0.76 g, the estimated heat changes were at 346 °C (619.15 K). The thermal properties shows the $La_{61.4}Al_{15.9}Ni_{11.35}Cu_{11.35}$ crystalline temperatures of 172.85 °C (446 K). Thus proving that the laser processing method can heat the La-based BMG samples to the crystalline region.

Table 7 The optimum parameters for the laser tracking of $La_{61.4}Al_{15.9}Ni_{11.35}Cu_{11.35}$ bulk metallic glass based on the FESEM observation

Laser power (W)	Frequency (kHz)	Speed (mm/s)
40–50	160–240	200–400

The research towards achieving the finest $La_{61.4}Al_{15.9}Ni_{11.35}Cu_{11.35}$ BMG FGM needs to be fine-tuned towards the specific application. Placing, gradient, pattern, or the depth of the needed FGM BMG needed to be tuned towards their explicit use. Other than that, the author's work is just the tip of the $La_{61.4}Al_{15.9}Ni_{11.35}Cu_{11.35}$ FGM BMG research and can be improved further.

4 Conclusion

This research presents the localised heating process of the BMG samples. The explored methods from the literature are the laser processing method. This process has proper proceeding research done on the BMG and is used as the reference. When the localised laser heating process was done, surpassing the eutectic point, coupled with the annealing process of the BMG samples with ambient temperature, the specific area of heating became crystalline, and a graded structure of BMG samples was created. The morphology of the heat-affected zones (HAZ) of $La_{62}Al_{14}Cu_{12}Ni_{12}$ BMG samples due to the laser processing at various parameters were observed and analysed in terms of the amorphicity and crystallinity. The ripple patterns structure reflected the crystallisation at the HAZ. The results concluded that for laser processing of the $La_{61.4}Al_{15.9}Ni_{11.35}Cu_{11.35}$ BMG samples' optimum ranges of power, frequency and speed are 40–50 W, 160–240 kHz and 200–400 mm/s, respectively. Thus the Lanthanum based FGM BMG was successfully created by the current work. The promising finding on the microstructural or morphology of the laser processing provides a good understanding for future advancement research on the $La_{61.4}Al_{15.9}Ni_{11.35}Cu_{11.35}$ BMG.

Acknowledgements The authors are grateful to the Ministry of Education Malaysia: FRGS/1/2017/TK05/UMP/01/1. Ministry of Science, Technology and Innovation (MOSTI), Malaysia SMD, Universiti Malaysia Pahang: 03-01-02-SF0257. The research work is strongly supported by the Advanced Structural Integrity and Vibration Research Group (ASIVR) and Structural Materials and Degradation (SMD) Focus Group, Faculty of Mechanical and Automotive Engineering Technology, University Malaysia Pahang. "Mohd Kamal bin Kamarulzaman" is the recipient of the UMP Post-Doctoral Fellowship in Research.

Declaration of Competing Interest The authors declare that they have no known competing financial interests or personal relationships that could have appeared to influence the work reported in this paper.

References

1. Chen M (2011) A brief overview of bulk metallic glasses. NPG Asia Mater 3(9):82–90. https://doi.org/10.1038/asiamat.2011.30
2. Ruhl RC (1967) Cooling rates in splat cooling. Mater Sci Eng 1(6):313–320. https://doi.org/10.1016/0025-5416(67)90013-4

3. Halim Q, Mohamed NAN, Rejab MRM, Naim WNWA, Ma Q (2021) Metallic glass properties, processing method and development perspective: a review. Int J Adv Manuf Technol. https://doi.org/10.1007/s00170-020-06515-z
4. Chen HS, Turnbull D (1969) Formation, stability and structure of palladium-silicon based alloy glasses. Acta Metall 17(8):1021–1031. https://doi.org/10.1016/0001-6160(69)90048-0
5. Argon AS (1979) Plastic deformation in metallic glasses. Acta Metall 27(1):47–58. https://doi.org/10.1016/0001-6160(79)90055-5
6. Spaepen F (1977) A microscopic mechanism for steady state inhomogeneous flow in metallic glasses. Acta Metall 25(4):407–415. https://doi.org/10.1016/0001-6160(77)90232-2
7. Inoue A, Wang XM, Zhang W (2008) Developments and applications of bulk metallic glasses. Rev Adv Mater Sci 18(1):1–9
8. Takeuchi A, Yubuta K, Makino A, Inoue A (2009) Evaluation of glass-forming ability of binary metallic glasses with liquidus temperature, crystallographic data from binary phase diagrams and molecular dynamics simulations. J Alloy Compd 483(1–2):102–106. https://doi.org/10.1016/j.jallcom.2008.07.186
9. Peker A, Johnson WL (1993) A highly processable metallic glass: $Zr_{41.2}Ti_{13.8}Cu_{12.5}Ni_{10.0}Be_{22.5}$. Appl Phys Lett 63(17):2342–2344. http://doi.org/10.1063/1.110520
10. Ouyang D, Li N, Xing W, Zhang J, Liu L (2017) 3D printing of crack-free high strength Zr-based bulk metallic glass composite by selective laser melting. Intermetallics 90:128–134. https://doi.org/10.1016/j.intermet.2017.07.010
11. Halim Q, Mohamed NAN, Rejab MRM, Naim WNWA, Ma Q (2021) Metallic glass properties, processing method and development perspective: a review. Int J Adv Manuf Technol 112(5):1231–1258. https://doi.org/10.1007/s00170-020-06515-z
12. Schroers J, Johnson WL (2004) Ductile bulk metallic glass. Phys Rev Lett 93(25):255506. https://doi.org/10.1103/PhysRevLett.93.255506
13. Cao JD, Kirkland NT, Laws KJ, Birbilis N, Ferry M (2012) Ca-Mg-Zn bulk metallic glasses as bioresorbable metals. Acta Biomater 8(6):2375–2383. https://doi.org/10.1016/j.actbio.2012.03.009
14. Pilarczyk W (2018) Structure and properties of Zr-based bulk metallic glasses in As-cast state and after laser welding. Materials (Basel) 11(7). http://doi.org/10.3390/ma11071117
15. Das J, Tang MB, Kim KB, Theissmann R, Baier F, Wang WH, Eckert J (2005) "Work-hardenable" ductile bulk metallic glass. Phys Rev Lett 94(20):205501. https://doi.org/10.1103/PhysRevLett.94.205501
16. Rizzi P, Habib A, Castellero A, Battezzati L (2013) Ductility and toughness of cold-rolled metallic glasses. Intermetallics 33:38–43. https://doi.org/10.1016/j.intermet.2012.09.026
17. Kolodziejska JA, Kozachkov H, Kranjc K, Hunter A, Marquis E, Johnson WL, Flores KM, Hofmann DC (2016) Towards an understanding of tensile deformation in Ti-based bulk metallic glass matrix composites with BCC dendrites. Sci Rep 6:22563. https://doi.org/10.1038/srep22563
18. Zhai H, Wang H, Liu F (2016) A strategy for designing bulk metallic glass composites with excellent work-hardening and large tensile ductility. J Alloy Compd 685:322–330. https://doi.org/10.1016/j.jallcom.2016.05.290
19. Scudino S, Bian JJ, Shakur Shahabi H, Sopu D, Sort J, Eckert J, Liu G (2018) Ductile bulk metallic glass by controlling structural heterogeneities. Sci Rep 8(1):9174. https://doi.org/10.1038/s41598-018-27285-5
20. Ekambaram R, Thamburaja P, Yang H, Li Y, Nikabdullah N (2010) The multi-axial deformation behavior of bulk metallic glasses at high homologous temperatures. Int J Solids Struct 47(5):678–690. https://doi.org/10.1016/j.ijsolstr.2009.11.008
21. Li XP, Kang CW, Huang H, Sercombe TB (2014) The role of a low-energy–density re-scan in fabricating crack-free $Al_{85}Ni_5Y_6Co_2Fe_2$ bulk metallic glass composites via selective laser melting. Mater Des 63:407–411. https://doi.org/10.1016/j.matdes.2014.06.022
22. Li N, Zhang J, Xing W, Ouyang D, Liu L (2018) 3D printing of Fe-based bulk metallic glass composites with combined high strength and fracture toughness. Mater Des 143:285–296. https://doi.org/10.1016/j.matdes.2018.01.061

23. Dong F, He M, Zhang Y, Wang B, Luo L, Su Y, Yang H, Yuan X (2019) Investigation of shear transformation zone and ductility of Zr-based bulk metallic glass after plasma-assisted hydrogenation. Mater Sci Eng A 759:105–111. https://doi.org/10.1016/j.msea.2019.05.027
24. Lu Y, Huang Y, Wu J (2018) Laser additive manufacturing of structural-graded bulk metallic glass. J Alloy Compd 766:506–510. https://doi.org/10.1016/j.jallcom.2018.06.259
25. Lu Y, Huang Y, Wu J, Lu X, Qin Z, Daisenberger D, Chiu Y-L (2018) Graded structure of laser direct manufacturing bulk metallic glass. Intermetallics 103:67–71. https://doi.org/10.1016/j.intermet.2018.10.005
26. Shin H-S, Jeong Y-J, Choi H-Y, Kato H, Inoue A (2007) Joining of Zr-based bulk metallic glasses using the friction welding method. J Alloy Compd 434–435:102–105. https://doi.org/10.1016/j.jallcom.2006.08.129
27. Chen B, Shi TL, Li M, Yang F, Yan F, Liao GL (2014) Laser welding of annealed $Zr_{55}Cu_{30}Ni_5Al_{10}$ bulk metallic glass. Intermetallics 46:111–117. https://doi.org/10.1016/j.intermet.2013.11.008
28. Chen B, Shi T, Li M, Wen C, Liao G (2015) Crystallization of $Zr_{55}Cu_{30}Al_{10}Ni_5$ bulk metallic glass in laser welding: simulation and experiment. Adv Eng Mater 17(4):483–490. https://doi.org/10.1002/adem.201400145
29. Kumar R, Kumar R, Chattopadhyaya S, Ghosh A, Kumar A (2015) Friction stir welding of BMG's: a review
30. Zhang H, Lu Y, Huang Y, Feng A, Qin Z, Lu X (2015) Joining of $Zr_{51}Ti_5Ni_{10}Cu_{25}Al_9$ BMG to aluminum alloy by friction stir welding. Vacuum 120:47–49. https://doi.org/10.1016/j.vacuum.2015.06.020
31. Huang Y, Xue P, Guo S, Wu Y, Cheng X, Fan H, Ning Z, Cao F, Xing D, Sun J, Liaw PK (2016) Liquid-solid joining of bulk metallic glasses. Sci Rep 6:30674. https://doi.org/10.1038/srep30674
32. Kim J, Lee T (2017) Brazing method to join a novel $Cu_{54}Ni_6Zr_{22}Ti_{18}$ bulk metallic glass to carbon steel. Sci Technol Weld Joining 22(8):714–718. https://doi.org/10.1080/13621718.2017.1306155
33. Halim Q, Nikabdullah N, Rejab MRM, Rashidi M (2020) Fracture response of $La_{61.4}Al_{15.9}Ni_{11.35}Cu_{11.35}$ bulk metallic glass subjected to quasi-static compression loading. Mater Today Proc 27:1761–1767. https://doi.org/10.1016/j.matpr.2020.03.662
34. Williams E, Lavery N (2017) Laser processing of bulk metallic glass: a review. J Mater Process Technol 247:73–91. https://doi.org/10.1016/j.jmatprotec.2017.03.034
35. Williams E, Brousseau EB (2016) Nanosecond laser processing of $Zr_{41.2}Ti_{13.8}Cu_{12.5}Ni_{10}Be_{22.5}$ with single pulses. J Mater Process Technol 232:34–42. https://doi.org/10.1016/j.jmatprotec.2016.01.023
36. Li B, Li ZY, Xiong JG, Xing L, Wang D, Li Y (2006) Laser welding of $Zr_{45}Cu_{48}Al_7$ bulk glassy alloy. J Alloy Compd 413(1–2):118–121. https://doi.org/10.1016/j.jallcom.2005.07.005
37. Ikutomo R, Tsujikawa M, Hino M, Kimura H, Yubuta K, Inoue A (2013) Crystallisation by laser for Zr based bulk metallic glass. Int J Cast Met Res 21(1–4):148–151. https://doi.org/10.1179/136404608x361855
38. Jiang MQ, Wei YP, Wilde G, Dai LH (2015) Explosive boiling of a metallic glass superheated by nanosecond pulse laser ablation. Appl Phys Lett 106(2). http://doi.org/10.1063/1.4905928
39. Best JP, Ast J, Li B, Stolpe M, Busch R, Yang F, Li X, Michler J, Kruzic JJ (2020) Relating fracture toughness to micro-pillar compression response for a laser powder bed additive manufactured bulk metallic glass. Mater Sci Eng A 770. https://doi.org/10.1016/j.msea.2019.138535
40. Liu WD, Ye LM, Liu KX (2011) Micro-nano scale ripples on metallic glass induced by laser pulse. J Appl Phys 109(4):043105–043109. http://doi.org/10.1063/1.3552914
41. Wessels V, Grigoryev A, Dold C, Wyen C-F, Roth R, Weingärtner E, Pude F, Wegener K, Löffler JF (2012) Abrasive waterjet machining of three-dimensional structures from bulk metallic glasses and comparison with other techniques. J Mater Res 27(8):1187–1192. https://doi.org/10.1557/jmr.2012.36

42. Zhang Y, Lin X, Wang L, Wei L, Liu F, Huang W (2015) Microstructural analysis of $Zr_{55}Cu_{30}Al_{10}Ni_5$ bulk metallic glasses by laser surface remelting and laser solid forming. Intermetallics 66:22–30. https://doi.org/10.1016/j.intermet.2015.06.007
43. Windl W (2016) Development of compositionally graded metallic glass alloys with desirable properties